

CHEMISTRY

AN **ASIAN** JOURNAL

www.chemasianj.org

Accepted Article

Title: Modulation of Crystal Packing via the Tuning of Peripheral Functionality for a Family of Dinuclear Mesocates

Authors: Ben H Wilson and Paul E Kruger

This manuscript has been accepted after peer review and appears as an Accepted Article online prior to editing, proofing, and formal publication of the final Version of Record (VoR). This work is currently citable by using the Digital Object Identifier (DOI) given below. The VoR will be published online in Early View as soon as possible and may be different to this Accepted Article as a result of editing. Readers should obtain the VoR from the journal website shown below when it is published to ensure accuracy of information. The authors are responsible for the content of this Accepted Article.

To be cited as: *Chem. Asian J.* 10.1002/asia.202000686

Link to VoR: <https://doi.org/10.1002/asia.202000686>

A Journal of



A sister journal of *Angewandte Chemie*
and *Chemistry – A European Journal*

WILEY-VCH

FULL PAPER

Modulation of Crystal Packing via the Tuning of Peripheral Functionality for a Family of Dinuclear Mesocates

Benjamin H. Wilson^{*[a,b]} and Paul E. Kruger^[a]

Abstract: A family of four novel pyrazinyl-hydrazone based ligands have been synthesized with differing functionality at the 5-position of the central aromatic ring. Previous work has shown such ligands to form dinuclear triple mesocates which pack to form hexagonal channels capable of gas sorption. The effect of the peripheral functionality of the ligand on the crystal packing was investigated by synthesizing complexes **1** to **4** which feature amino, bromo, iodo and methoxy substituents respectively. Complexes **1** to **3** crystallized in the same hexagonal space group $P6_3/m$ and featured 1D channels. However, on closer inspection while the packing of **1** is mediated by hydrogen bonding interactions, the packing of complexes **2** and **3** are not, due to a subtly different π - π stacking interaction enforced by the halogen substituent. The more bulky nature of the methoxy substituent of **4** results in the complex crystallizing in the triclinic space group $P-1$, featuring an entirely different crystal packing.

Introduction

Crystal engineering describes the use of supramolecular interactions to design materials with desirable properties.¹ One strategy is to utilise molecular tectons designed to form specific, spatially oriented intermolecular interactions and therefore assemble in a controlled manner.² This approach can be utilised to engineer molecular materials containing *extrinsic* porosity,³ exemplified by the growing number of Hydrogen Bonded Organic Frameworks (HOFs)⁴ and other Molecular Porous Materials (MPMs)^{3,5}. Discrete metallo-supramolecular assemblies are an attractive supramolecular tecton for building framework materials as they provide a scaffold for the controlled orientation of hydrogen bonding moieties.⁶ Framework materials based on molecular species often suffer from instability unlike Metal Organic Frameworks (MOFs)⁷ due to the weaker nature of the network forming interactions. However, molecular species have enhanced solubility making them solution processable.⁸ Due to the weaker nature of hydrogen bonds compared to coordinate

bonds,⁹ systematically altering peripheral functional groups while retaining an isostructural framework is challenging unlike in MOFs.¹⁰ Therefore, a system in which peripheral functionality of the ligand can be modulated without significantly altering the crystal packing is highly desirable. We recently reported a dinuclear triple mesocate incorporating a bispyrazinyl-hydrazone ligand.^{5b} The mesocate complex featured strong hydrogen bonding and π - π stacking interactions between the hydrazone and pyrazine moieties on neighboring complexes. This resulted in the mesocates packing such that microporous hexagonal channels were formed. Removal of the solvent molecules from these channels resulted in a porous material which exhibited selective carbon dioxide sorption over nitrogen rationalised by the presence of fluorinated anions in the pores.¹¹ In this work, the peripheral functionality of the ligand is modified to investigate the effect on the crystal packing to assess the reliability of this mesocate tecton. The 5-position of the central aromatic ring of this family of ligands can be readily functionalized via a number of commercially available or readily synthesized isophthalic acid precursors. We report the synthesis of four novel bispyrazinyl-hydrazone ligands with amino, bromo, iodo and methoxy and their resulting Fe(II) complexes and seek to rationalize the differences in the crystal packing.

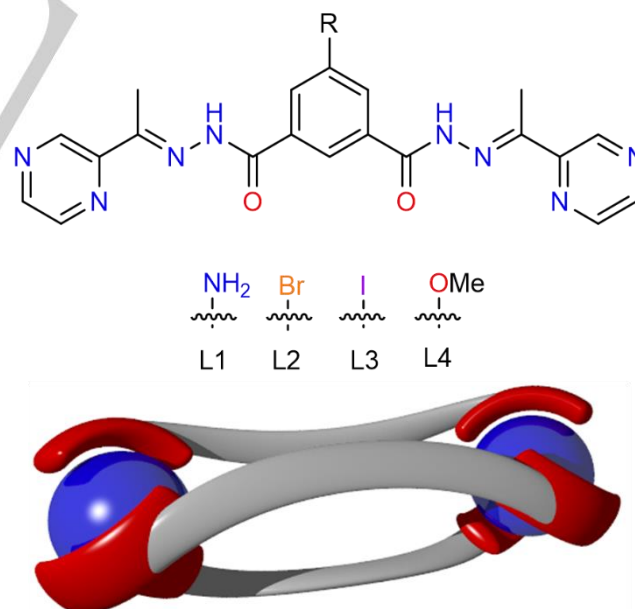


Figure 1. (top) The bispyrazinyl-hydrazone ligands for which the 5 position of the central aromatic ring (R) has been functionalised with amino, bromo, iodo and methoxy substituents. (bottom) A schematic representation of the dinuclear triple mesocate formed with the family of ligands described above.

[a] B. H. Wilson, Prof. P. E. Kruger
MacDiarmid Institute for Advanced Materials and Nanotechnology,
School of Physical and Chemical Sciences
University of Canterbury
Christchurch 8041, New Zealand
[b] B. H. Wilson
Department of Chemistry and Biochemistry
University of Windsor
Windsor, Ontario, N9B 3P4, Canada
E-mail: bwilson@uwindsor.ca

Supporting information for this article is given via a link at the end of the document

Results and Discussion

FULL PAPER

Ligands **L1** to **L4** formed complexes **1** to **4** with the molecular formula $[\text{Fe}_2(\text{L})_3](\text{BF}_4)_4$. Complexes **1** and **2** were synthesized by stirring the appropriate ligand and $\text{Fe}(\text{BF}_4)_2 \cdot 6\text{H}_2\text{O}$ in nitromethane in a stoichiometry of 3:2. The poor solubility of ligands **L3** and **L4** in nitromethane required complexes **3** and **4** to first be synthesized in acetonitrile, followed by subsequent crystallization from nitromethane. The effect on the crystal packing by modulating the peripheral functionality was then investigated (figure 1).

Complex 1

Vapor diffusion of toluene into a dark red nitromethane solution of complex **1** gave red rod-shaped crystals. Single crystal X-ray diffraction was conducted at 120 K and the data was solved and refined in the same hexagonal space group as our previously reported complex; $P6_3/m$.^{5b} Much like the original complex, the asymmetric unit contained one half of a ligand fragment coordinated to one third of an Fe(II) center in a bidentate fashion. The two crystallographically unique Fe-N bonds are 1.946(4) Å (Fe1-N2) and 1.962(4) Å (Fe1-N3) and indicate that the Fe(II) center is in the low spin state at 120 K (figure S1). The pitch of the mesocate runs parallel to the crystallographic c-axis and measures 11.625(2) Å and is congruent with a 3-fold roto-inversion axis. The action of the aforementioned roto-inversion axis followed by reflection about a mirror plane perpendicular to the crystallographic c-axis generates the complete dinuclear triple mesocate structure. The carbonyl functionality is not coplanar with the central phenyl ring and exhibits an out of plane twist of 26.4(7)° (measured as the C13-C12-C14-C15 torsion). This

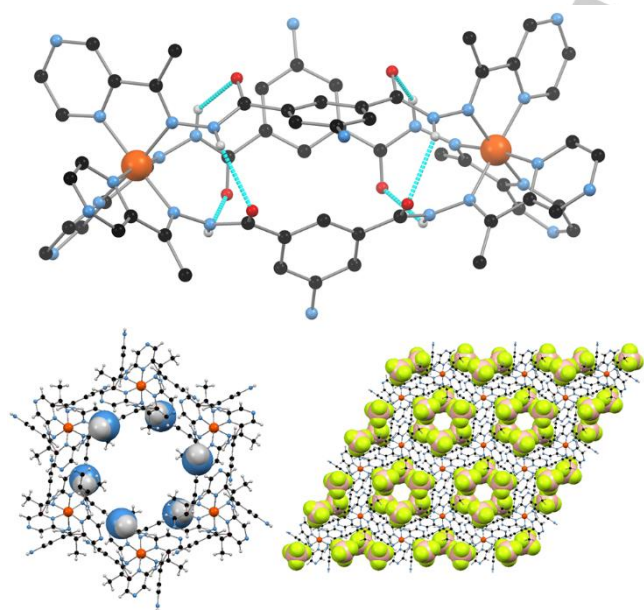


Figure 2. (top) The dinuclear triple mesocate structure of **1** showing the hydrazide hydrogen bonding interactions with the carbonyl oxygen atoms in blue. (left) View of the crystal packing of **1** down the crystallographic c-axis showing the hexagonal 1-D channel with the amine substituents highlighted in space filling representation with the tetrafluoroborate anions. (right) The crystal packing viewed down the crystallographic c-axis showing the tetrafluoroborate anions lining the channel in space filling representation.

results in the formation of intramolecular hydrogen bonding interactions between the carbonyl oxygen atom and a hydrazide group on an adjacent (inter-strand) ligand, O13...H11(N11), 2.328(3) Å, 127.7(3)° (figure 2, table S3). These hydrogen bonding interactions are reinforced by three crystallographically identical reciprocal edge-to-face C-H... π interactions, C15-H15... π (center-of-ring) 2.928(4) Å, 152.7(5)° (figure S2, table S4). The mesocate structure is predominantly favored by the 1,3-substitution pattern on the central phenyl spacer which induced the bidentate coordination sites to be orientated in the same direction.¹² The intra-strand hydrogen bonding interactions further support the formation of the mesocates structure. The C-H... π interactions occur as a result of the strained ligand conformation adopted upon the mesocate formation enforced by the 1,2-substitution pattern on the central phenyl spacer. The supramolecular interactions occurring between the mesocates in **1** are analogous to that of our previously reported complex, the most prominent being a hydrogen bonding interaction between the N6 atom of the pyrazine ring and the hydrazide moieties on neighboring mesocates N11-H11...N6, 2.240(5) Å (figure S4, table S5). An off-set π - π stacking interaction between the pyrazine rings of neighboring mesocates is also evident with a centroid-centroid separation of 3.719(4)Å (figure S4, table S6) which extends down the crystallographic c-axis. This gives rise to the formation of large hexagonal channels parallel to the crystallographic c-axis (figure 2, figure S4-5). The Fe1-Fe1' spacing of adjacent mesocates forming a channel is 8.3172(6) Å the channel diameter at the closest contact is ca. 6.09 Å. The tetrafluoroborate anions line the sides of the 1-D channels, disordered over two positions. Due to the high symmetry of the space group and the disorder exhibited by the solvent molecules, they were unable to be modelled satisfactorily and therefore the SQUEEZE¹³ function of PLATON¹⁴ was applied. The solvent accessible void was calculated to be 1031 Å³ and contained 330 electrons, corresponding to 145 electrons per mesocate. Therefore, the contents of the channel can be approximated as three toluene molecules (150 electrons). TGA analysis showed a 4.97% weight loss between 20 and 152 °C, which is approximates one molecule of toluene which constitutes 5.1% of the mass of 1-C₆H₇, in agreement with the elemental analysis. Thermogravimetric analysis also reveals that **1** is stable until 200 °C after which there is a rapid decrease in the mass due to decomposition. The addition of the amino substituent has had a negligible effect on the crystal packing of **1** compared to our previously reported complex,^{5b} indicating the inherent stability of the complementary hydrogen bonding and π - π stacking interactions.

Complex 2

Vapor diffusion diisopropyl ether into a dark red nitromethane solution of complex **2** gave red rod-shaped crystals. Single crystal X-ray diffraction was conducted at 120 K and the data was solved and refined in the same hexagonal space group as **1**, $P6_3/m$, however with a longer crystallographic c-axis dimension. The asymmetric unit contained one half of a ligand fragment coordinated to one third of an Fe(II) center in a bidentate fashion. The two crystallographically unique Fe-N bonds are 1.95(1) Å (Fe1-N2) and 1.953(9) Å (Fe1-N3) and indicate that the Fe(II)

For internal use, please do not delete. Submitted_Manuscript

FULL PAPER

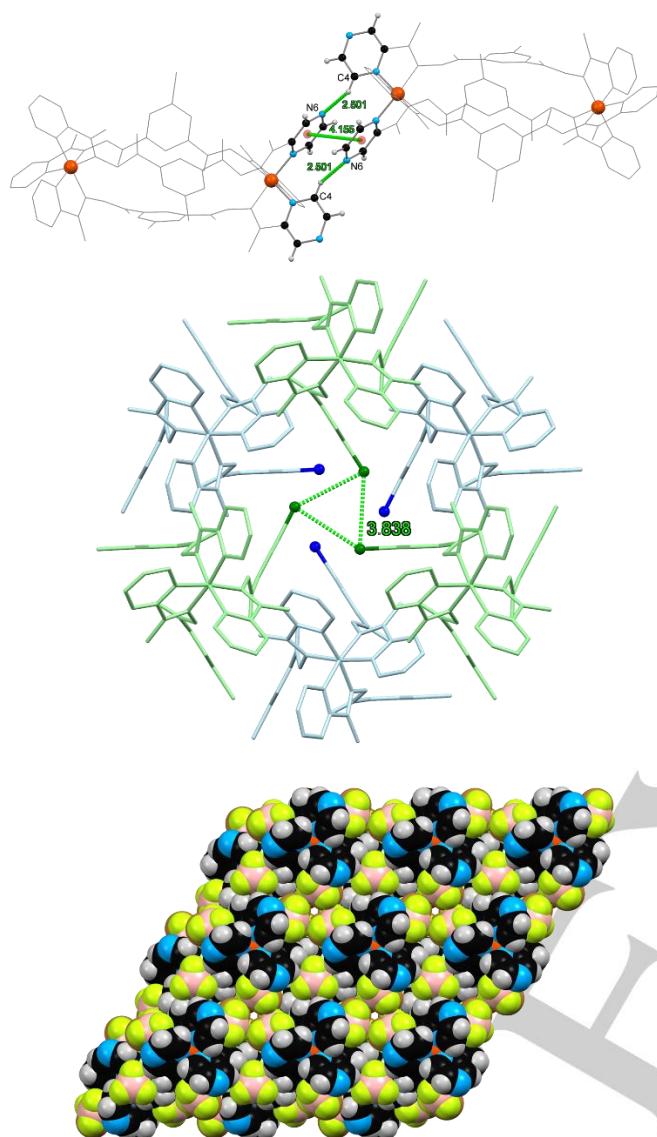


Figure 3. (top) The N6...H4(C4) interactions and the offset π ... π interaction are shown in green. The π ... π interaction is measured via the centroid...centroid (red) separations. (middle) The crystal packing of **2** viewed down the crystallographic *c*-axis. The trimeric Br...Br halogen bonding interactions are shown in green. The three mesocates in pale green sit above the three mesocates shown in pale blue. Hydrogen atoms and tetrafluoroborate anions omitted for clarity. (bottom) Crystal packing of **2** in space filling representation highlighting the apparent lack of 1D channels down the crystallographic *c*-axis.

center is in the low spin state at 120 K (figure S6). The pitch of the mesocate runs parallel to the crystallographic *c*-axis and measures 11.599(5) Å and is congruent with a 3-fold roto-inversion axis. The action of the roto-inversion axis followed by reflection about a mirror plane perpendicular to the crystallographic *c*-axis generates the complete dinuclear triple mesocate structure (figure S7). The carbonyl functionality is not coplanar with the central phenyl ring and exhibits an out of plane

twist of 23(2)° (measured as the C13-C12-C14-C15 torsion). This results in the formation of intramolecular hydrogen bonding interactions between the carbonyl oxygen atom and a hydrazide group on an adjacent (inter-strand) ligand, O13...H11(N11), 2.370(8) Å, 123.4(7)° (table S3). These hydrogen bonding interactions are reinforced by three crystallographically identical reciprocal edge-to-face C-H... π interactions, C15-H15... π (center-of-ring) 2.882(7) Å, 148.8(1)° (figure S7, table S4). The combination of the hydrogen bonding and C-H... π interactions result from the mesocate structure enforced by the 1,3-substitution pattern on the central phenyl spacer as discussed for **1**.

On first appearance, the packing of **2** seems analogous to **1**. When viewed down the crystallographic *c*-axis a similar hexagonal packing occurs (figure 3, figure S8), however with a more compact 1-D channel. On closer inspection, the pyrazine rings π - π stack upon one another with a noticeably larger centroid separation of 4.16(1) Å (table S6). This is due to the stacking interaction occurring between the opposite faces of the pyrazine rings in comparison to **1**. A direct consequence of this change in π - π stacking is that the pyrazine-hydrazide hydrogen bond, observed in **1**, does not form. Instead a weak C-H...N interaction between C4 and N6 of neighboring pyrazine rings occurs while the hydrazide moieties form a hydrogen bonding interaction with the tetrafluoroborate anions (figure 3, figure S6, table S5). The Fe1...Fe1' spacing of the Fe(II) centers coordinated to these pyrazine rings also increases to 9.410(3) Å. The more expanded packing along the crystallographic *c*-axis can be attributed to the incorporation of the bromine functionality on C17. These bromine atoms are orientated into the hexagonal channel towards one another with a Br18...Br18 separation of 3.837(4) Å, 144.1(7)° resulting in the formation of a trimeric type II halogen bond (figure 3).¹⁵ This more expanded packing of the mesocates propagates along the *c*-axis resulting in a significantly long *c*-axis dimension for **2** of 34.658(6) Å in comparison to **1**, 24.854(2) Å. There is also a small decrease in the crystallographic *a* and *b*-axis from 14.340(1) Å for **1** to 12.928(3) Å for **2**. This compression in the crystallographic *a* and *b*-axis manifests itself as a more compact 1-D channel with a diameter at the closest contact of ca. 4.77 Å. The tetrafluoroborate anions line the sides of the noticeably thinner channel. As with **1**, disordered solvent molecules occupy the middle of the channel which, due to the high symmetry of the space group, are unable to be modelled satisfactorily and therefore the SQUEEZE¹³ function of PLATON¹⁴ was applied. The solvent accessible void was calculated to be 1157 Å³ and calculated to contain 362 electrons, corresponding to 181 electrons per mesocate. Therefore, the contents of the channel can be approximated as two nitromethane molecule and two diisopropyl ether molecules (148 electrons). Thermogravimetric analysis reveals a weight loss of 5.91% between 26 and 133 °C which corresponds to the loss of one diisopropyl ether molecule which constitutes 5.1% of the mass of **2**, C₆H₁₄O and is also observed in the elemental analysis. Thermogravimetric analysis also reveals that **2** is stable until 200 °C after which there is a rapid decrease in the mass due to decomposition. While a similar hexagonal type packing to **1** is observed, the incorporation of the bromo substituent results in a halogen bonding interaction which

For internal use, please do not delete. Submitted_Manuscript

FULL PAPER

prevents the hydrogen bonding interaction of **1** occurring. This results expansion and contraction along the crystallographic *c*-axis and crystallographic *a* and *b*-axis respectively giving rise to a more compact 1-D channel.

Complex 3

Vapour diffusion of diisopropyl ether into a dark red nitromethane solution of complex **3** gave red prismatic crystals. Single crystal X-ray diffraction was conducted at 120 K and the data was solved and refined in the same hexagonal space group as **1**, $P6_3/m$, however with a longer crystallographic *c*-axis dimension. The asymmetric unit contained one half of a ligand fragment coordinated to one third of an Fe(II) centre in a bidentate fashion. The two crystallographically unique Fe-N bonds are 1.958(7) Å (Fe1-N2) and 1.955(7) Å (Fe1-N3) and indicate that the Fe(II) centre is in the low spin state at 120 K (figure S10). The pitch of the mesocate runs parallel to the crystallographic *c*-axis and measures 11.622(4) Å and is congruent with a 3-fold roto-inversion axis (figure S11). The action of the aforementioned roto-inversion axis followed by reflection about a mirror plane perpendicular to the crystallographic *c*-axis generates the complete dinuclear triple mesocate structure. The carbonyl functionality is not coplanar with the central phenyl ring and exhibits an out of plane twist of 22.9(9)° (measured as the C13-C12-C14-C15 torsion). This results in the formation of intramolecular hydrogen bonding interactions between the carbonyl oxygen atom and a hydrazide group on an adjacent (inter-strand) ligand, O13...H11(N11), 2.942(9) Å, 125.0(6)° (figure 4, table S3). These hydrogen bonding interactions are reinforced by three crystallographically identical reciprocal edge-to-face C-H... π interactions, C15-H15... π (centre-of-ring) 2.850(5) Å, 147.3(7)° (figure S11, table S4).

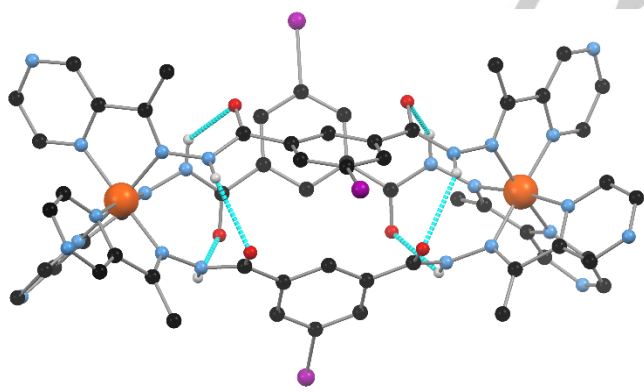


Figure 4. The dinuclear triple mesocate structure of **3** showing the hydrazide hydrogen bonding interactions with the carbonyl oxygen atoms in blue. Hydrogen atoms not participating in hydrogen bonding interactions and tetrafluoroborate anions are omitted for clarity.

The combination of the hydrogen bonding and C-H... π interactions result from the mesocate structure enforced by the 1,3-substitution pattern on the central phenyl spacer as discussed for **1** and **2**. The similar nature of the ligand substituent to **2** results in the complex adopting an isomorphous crystal packing (figure

S14-15). The π - π stacking of the pyrazine rings of neighboring complexes upon

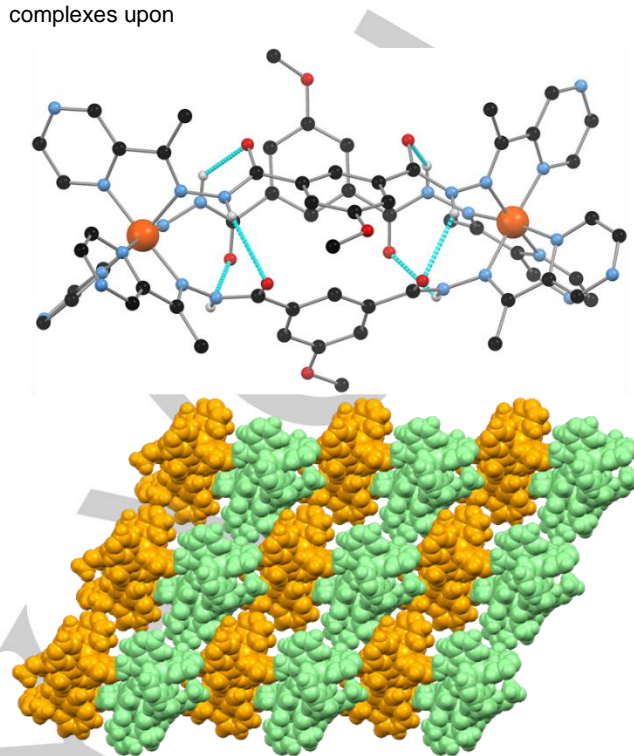


Figure 5. (top) The dinuclear triple mesocate structure of **3** showing the hydrazide hydrogen bonding interactions with the carbonyl oxygen atoms in blue. Hydrogen atoms not participating in hydrogen bonding interactions and tetrafluoroborate anions are omitted for clarity. (bottom) The crystal packing viewed down the crystallographic *c*-axis. The complexes shown in green interact with the neighbouring complexes shown in orange via non-conventional O...H(C) interactions.

one another with a centroid...centroid separation of 4.182(7) Å, is noticeably longer than that of **1** and similar to that of **2** (figure S10). Much like **2**, the opposite faces of the pyrazine rings are involved in this stacking interaction, resulting in the absence of the pyrazine-hydrazide hydrogen bonding interaction. Analogous to **2**, a weak C-H...N interaction between C4 and N6 of neighboring pyrazine rings occurs, while the hydrazide moieties form a hydrogen bonding interaction with the tetrafluoroborate anions (figure S13, table S5-S6). The Fe1...Fe1 spacing of the Fe(II) centers coordinated to these pyrazine rings is 9.424(2) Å similar to that of **2**. The iodo substituents are orientated into the hexagonal channel towards one another with an I18...I18 separation of 3.985(2) Å resulting in a trimeric type II halogen bond analogous to **2** (figure S13).¹⁵ Unlike the bromo substituents of **2**, the iodine atoms are modeled as disordered over two positions with an occupancy ratio of 9:1.

This more expanded packing of the mesocates propagates along the *c*-axis resulting in a significantly long *c*-axis dimension for **3** of 34.658(6) Å in comparison to **1**, 24.854(2) Å and similar to the values for **2**. Likewise, as for **2**, there is also a small decrease in the crystallographic *a* and *b*-axis from 14.340(1) Å for **1** to 12.928(3) Å for **3**. The more compact 1D channel of **3** possesses

For internal use, please do not delete. Submitted_Manuscript

FULL PAPER

a diameter at the closest contact of ca. 3.99 Å. The tetrafluoroborate anions line the sides of the noticeably thinner channel in a manner analogous to **2**. As with **1** and **2**, disordered solvent molecules occupy the middle of the channel which, due to the high symmetry of the space group, are unable to be modelled satisfactorily and therefore the SQUEEZE¹³ function of PLATON¹⁴ was applied. The solvent accessible void was calculated to be 1129 Å³ and calculated to contain 312 electrons, corresponding to 156 electrons per mesocate. Therefore, the contents of the channel can be approximated as two diisopropyl ether and one water molecule (158 electrons). Thermogravimetric analysis reveals a weight loss of 4.81% between 41 and 177 °C which corresponds to the loss of one diisopropyl ether molecule which constitutes 4.8% of the mass of **3**·C₆H₁₄O and is also observed in the elemental analysis. Thermogravimetric analysis also reveals that the complex is stable until 200 °C after which there is a rapid decrease in the mass due to decomposition.

Complex 4

Vapor diffusion of diisopropyl ether into a dark red nitromethane solution of **4** gave red plate crystals. Single crystal X-ray diffraction was conducted at 120 K and the data was solved and refined in the triclinic space group *P*-1. The asymmetric unit contained three ligands and two crystallographically unique Fe(II) centers (figure S16). The ligands coordinated to the Fe(II) centers in a bidentate manner, forming a dinuclear triple mesocate. The Fe-N bond lengths indicate that both Fe(II) centers exist in the low spin state at 120 K (table S2). The pitch of the mesocate measures 11.624(1) Å and the axis is no longer coincident with the crystallographic *c*-axis. Like the previous complexes, the carbonyl functionality is not coplanar with the central aromatic rings of the ligands and with torsion angles ranging from 19.5(5) to 23.0(6)°. As with the previously discussed complexes, intramolecular hydrogen bonding interactions between the carbonyl oxygen atom and a hydrazide group on an adjacent (inter-strand) ligand, O...H(N), with values ranging from 2.856(5) to 3.098(4) Å (figure 5, table S3). These hydrogen bonding interactions are reinforced by three reciprocal edge-to-face C-H... π interactions, C15-H15... π (center-of-ring) with values ranging from 2.834(2) Å to 2.900(2) Å as observed in **1** to **3** (figure S18, table S4). The inclusion of the methoxy functionality make the complex sufficiently sterically encumbered such that the packing observed for **1** or **2** and **3** cannot occur. Instead the hydrazide moieties participate in hydrogen bonding interactions with the tetrafluoroborate anions and a nitromethane solvent molecule (figure S18, table S5). There are only weak supramolecular interactions between neighboring mesocates in the form of non-conventional hydrogen bonds. There are two types of C-H...O interactions between the acetyl group of the ligand on one mesocate and the carbonyl oxygen and the methoxy oxygen atoms on a neighboring mesocate (figure S20). This interaction leads to the formation of supramolecular dimers, which pack end-on-end down the crystallographic *c*-axis (figure 5, figures S20-22). While some of the nitromethane solvent molecules were able to be modelled in the crystal structure, there remained a large amount of disordered solvent and therefore the SQUEEZE¹³ function of PLATON¹⁴ was applied. The solvent accessible void was calculated to be 1126 Å³ and calculated to

contain 345 electrons, corresponding to 173 electrons per helicate. The solvent content can therefore be approximated as two diisopropyl ether and two nitromethane molecules (180 electrons). Thermogravimetric analysis reveals a weight loss of 6.12% between 41 and 177 °C which corresponds to the loss of one diisopropyl ether and one water molecule which constitutes 6.4% of the mass of **4**·C₆H₁₄O·H₂O and is also observed in the elemental analysis. Thermogravimetric analysis also reveals that the complex is stable until 200 °C after which there is a rapid decrease in the mass due to decomposition. The incorporation of the sterically encumbered methoxy substituent prohibits the hexagonal type packing observed for **1** to **3** to occur, resulting in a less symmetrical packing arrangement adopted instead.

Comparison of complexes 1 to 4

Structures 1-3 all crystallize in the same hexagonal space group *P*6₃/*m* resulting in hexagonal channels parallel to the crystallographic *c*-axis. However, only **1** has identical crystal packing to that of our previously reported structure, as the amino substituent plays no significant structure direction role. For **2** and **3**. The propensity of the halogen functionalities to form halogen bonds alters the crystal packing subtly. Looser packing of the mesocates in **2** and **3** results in a significantly longer *c*-axis while the *a* and *b* axis are slightly smaller than those of **1** and our previously reported complex. When a more bulky substituent, that cannot form stabilizing interactions with substituents on neighboring mesocates, is employed the complexes pack in an entirely different manner. The complex now crystallizes in the triclinic space group *P*-1 and the hexagonal channels present in complexes **1** to **3** no longer occur. This change in the packing is proposed to be due to a steric effect, in contrast to **2** and **3** where it is proposed to be due to an electronic effect (halogen bonding). Computational chemistry is a complementary technique to single crystal X-ray diffraction which can provide further insight into how differing supramolecular interactions influence the 3D structure,²³ however, it is beyond the scope of this work.

Conclusions

A family of four novel pyrazinyl-hydrazone ligands have been synthesized with a variety of functionality at the 5-position of the central aromatic ring. When complexed with Fe(II), these ligands coordinate in an unusual bidentate manner resulting in the formation of dinuclear triple mesocates. While the variation of the substituents in the 5-position of the central aromatic ring, R, have no effect on the structure of the discrete complex formed, they have a significant influence on the crystal packing of the complex. This is observed for **4**, where the methoxy substituent has a major structure directing role. When R = NH₂, for **1**, the complexes form strong pyrazine-pyrazine π - π and pyrazine-hydrazone hydrogen bonds, resulting in the formation of hexagonal channels parallel to the *c*-axis. When R = Br or I for **2** and **3** respectively, the packing is subtly different. The π - π interactions of the pyrazine rings occur between the opposite faces and there are no pyrazine-hydrazone hydrogen bonds. It is proposed that the occurrence of halogen bonds between the Br or I substituents are responsible for the altered crystal packing. When R = OMe for **4** the complex adopts

For internal use, please do not delete. Submitted_Manuscript

FULL PAPER

an entirely different crystal packing and the hexagonal channels observed in the previous structures do not occur. As no prominent intermolecular interactions can be ascertained from the structure we postulate that the steric bulk of the methoxy substituent is responsible for the drastic change in the crystal packing. The variation of the peripheral functionality has provided insight into how different types of supramolecular interactions modulate the crystal packing whether it be a subtle or significant change.

Experimental Section

Materials and methods

All reagents were used as received without further purification from BDH and Sigma Aldrich. ^1H and ^{13}C -NMR measurements were carried out on an Agilent 400 MR spectrometer operating at 400 MHz for ^1H and 101 MHz for ^{13}C . Mass spectrometry analysis was obtained on a Bruker maXis 4G time of flight spectrometer. Infrared spectra were recorded on a Bruker ALPHA Platinum ATR FT-IR spectrometer in the range 400–4000 cm^{-1} . Elemental analysis for C, H and N were carried out at Campbell Micro Analytical Laboratories, Otago University, Dunedin. Difficulties were encountered in synthesizing the complexes in bulk quantities and the presence of impurities is reflected in the elemental analysis. However, as it is solely the crystal structure of interest, the elemental analyses obtained were deemed sufficient. Thermo gravimetric analysis was carried out on an Alphatech SDT Q600 TGA/DSC apparatus. The sample holder was alumina crucible and it was heated at 1°min^{-1} under a nitrogen flow of 100 mL min^{-1} . Single crystal X-ray diffraction was carried out on an Agilent Supernova with an Atlas CCD area detector using graphite-monochromatized Cu-K α ($\lambda = 1.54178 \text{ \AA}$) radiation. The structures were solved using intrinsic phasing with SHELXT¹⁶ and refined on Olex2¹⁷ using all data by full matrix least-squares procedures with SHELXT-97.¹⁸ Non-hydrogen atoms were refined with anisotropic displacement parameters. Hydrogen atoms were included in calculated positions with isotropic displacement parameters 1.2 times the isotropic equivalent of their carrier atoms. The functions minimized were $\sum_w(F_o^2 - F_c^2)$, with $w = [\sigma^2(F_o^2) + aP^2 + bP]^{-1}$, where $P = [\max(F_o^2) + 2F_c^2]/3$. CCDC 2008563 to 2008566 contain the supplementary crystallographic data for this paper. These data are provided free of charge by the Cambridge Crystallographic Data Centre. 5-Bromo isophthalic acid,¹⁹ dimethyl 5-bromo isophthalate,¹⁹ dimethyl 5-iodoisophthalate,²⁰ 5-Iodo isophthaloyl hydrazide²¹ and dimethyl 5-methoxy isophthalate²² were synthesised following literature procedures.

Synthesis of 5-Amino isophthaloyl hydrazide

Dimethyl 5-amino isophthalate (1 g, 4.8 mmol) was dissolved in ethanol (5 mL) at reflux. Hydrazine mono hydrate (1.9 mL, 38 mmol) was added and the resulting white suspension stirred at reflux overnight. After cooling to room temperature, the white precipitate was filtered and washed with ethanol (3x5 mL) and then diethyl ether (10 mL) to give a white powder (968 mg, 4.6 mmol, 96% yield). MP: $>300^\circ \text{C}$ $^1\text{H-NMR}$ ($\text{D}_6\text{-DMSO}$): 9.44 (2H, br., s), 7.29 (1H, s), 7.05 (2H, s), 5.39 (2H, s), 4.41 (4H, br., s) $^{13}\text{C-NMR}$ ($\text{D}_6\text{-DMSO}$): 167, 149, 135, 115, ν_{max} (cm^{-1}): 3416(w), 3303 (br., m), 3219 (br., w), 1667 (m), 1589 (s), 1516 (s), 1309 (m), 1076 (w), 1001 (w), 946 (m), 869 (m), 818 (w), 750 (w), 729 (m), 679 (m), 598 (w), 443 (m) ESI-MS: $[\text{C}_8\text{H}_{12}\text{N}_5\text{O}_2]^+$ calc. 210.0986, meas. 210.0988

Synthesis of L1

5-Amino isophthaloyl hydrazide (600 mg, 2.9 mmol) was stirred in ethanol (50 mL) at room temperature. 2-Acetyl pyrazine was added followed by a

catalytic amount of glacial acetic acid and the resulting white suspension stirred at reflux overnight. After cooling to room temperature, the precipitate was filtered and washed with ethanol (2x5 mL) the diethyl ether (2x5 mL) to give a white powder (1.2 g, 2.9 mmol, 100% yield) MP: $>300^\circ \text{C}$ ν_{max} (cm^{-1}): 3396 (w), 3165 (br., w), 2961 (br. w), 1645 (s), 1615 (s), 1518 (s), 1471 (w), 1424 (m), 1346 (m), 1330 (m), 1258 (s), 1172 (m), 1156 (m), 1141 (m), 1118 (w), 1085 (m), 1052 (w), 1013 (m), 986 (w), 899 (w), 880 (w), 855 (s), 802 (w), 716 (w), 731 (w), 687 (m), 662 (br., m), 573 (w), 481 (w), 464 (w) ESI-MS: $[\text{C}_{20}\text{H}_{20}\text{N}_9\text{O}_2]^+$ calc. 418.1735, meas. 418.1743

Synthesis of 5-bromo isophthaloyl hydrazide

5-Bromo dimethyl isophthalate (0.8 g, 2.9 mmol) was dissolved in ethanol (3 mL) heated at reflux to give a yellow solution. Hydrazine monohydrate was added (0.71 mL, 15 mmol) and the resulting yellow solution which formed a white precipitate after several hours. A further 3 mL of ethanol was added and the white suspension was heated at reflux overnight. The suspension was then cooled to room temperature and the white solid was separated by filtration and washed with ethanol (3x5 mL) then diethyl ether (2x10 mL) to give a white powder (0.78 g, 2.9 mmol, 100% yield). MP: 280°C $^1\text{H-NMR}$ ($\text{D}_6\text{-DMSO}$): 4.55 (br. s., 4 H) 8.08 (d, $J = 1.17 \text{ Hz}$, 2 H) 8.24 (d, $J = 1.56 \text{ Hz}$, 2 H) 9.93 (br. s., 2 H) $^{13}\text{C-NMR}$ ($\text{D}_6\text{-DMSO}$): 122, 126, 132, 136, 164 ν_{max} (cm^{-1}): 3290 (s), 3176 (w), 3071 (w), 1638 (s), 1618 (s), 1571 (m), 1512 (s), 1430 (w), 1340 (m), 1313 (m), 1267(w), 1117 (m), 1005 (m), 914 (w), 888 (m), 788 (w), 769 (w), 741 (m), 731 (m), 675 (s), 624 (s) ESI-MS: $[\text{C}_8\text{H}_{10}\text{BrN}_4\text{O}_2]^+$, meas. 272.9983, calc. 272.9982

Synthesis of L3

5-Bromo isophthaloyl hydrazide (0.703g, 2.57 mmol) was stirred in ethanol (50 mL) at room temperature. 2-Pyridinecarboxaldehyde (564 μL , 5.92 mmol) was added followed by two drops of glacial acetic acid. The resulting white suspension was heated overnight at reflux. Upon cooling to room temperature, the white precipitate was filtered and washed with ethanol (2x10 mL) and then diethyl ether (2x10 mL) to give a white powder (0.854 mg, 1.8 mmol, 74% yield). MP: $256\text{-}258^\circ \text{C}$ ν_{max} (cm^{-1}): 3220 (w, br.), 3053 (w, br.), 1649 (s), 1587 (w), 1544 (s), 1470 (m), 1430 (m), 1368 (m), 1341 (w), 1295 (s), 1274 (s), 1249 (s), 1167 (m), 1148 (m), 1064 (m), 994 (m), 951 (m), 890 (m), 785 (s), 753 (w), 729 (s) ESI-MS: $[\text{C}_{20}\text{H}_{18}\text{BrN}_8\text{O}_2]^+$ meas.451.0523, calc. 451.0513, $[\text{C}_{20}\text{H}_{19}\text{BrN}_8\text{O}_2]^{2+}$ meas. 227.0282 calc. 227.0283

Synthesis of L4

5-Iodo isophthaloyl hydrazide (400 mg, 1.2 mmol) was stirred in 25 mL ethanol at room temperature. 2-Acetyl pyrazine (351 mg, 2.9 mmol) was added followed by a catalytic amount of glacial acetic acid. The resulting white suspension was heated at reflux overnight. The suspension was filtered and washed with ethanol (2x5 mL) the diethyl ether (2x5 mL) to give an off-white powder (561 mg, 1.1 mmol, 92% yield). MP: $>300^\circ \text{C}$ ν_{max} (cm^{-1}): 3171 (br., w), 3019 (br., w), 1665 (m), 1646 (s), 1615 (w), 1537 (s), 1468 (m), 1422 (m), 1369 (m), 1304 (w) 1252 (m), 1171 (s) 1155 (m) 1118 (s) 1073 (m), 1047 (m), 1012 (w), 986 (m), 928 (w), 866 (w), 855 (m), 821 (m), 789 (w), 761 (w), 728 (w), 713 (m), 682 (m), 652 (br., m), 564 (w), 459 (m)

Synthesis of L4 5-methoxy isophthaloyl hydrazide

Dimethyl 5-hydroxy isophthalate (1.5 g, 6.7 mmol) was dissolved in ethanol (10 mL) at reflux. Hydrazine mono hydrate (1.95 mL, 40 mmol) was added and the resulting yellow solution heated at reflux overnight. During this time a white suspension form which was subsequently cooled to room temperature and then in the fridge for 15 minutes. The white precipitate

For internal use, please do not delete. Submitted_Manuscript

FULL PAPER

was filtered and washed with ethanol (2 mL) and diethyl ether (10 mL) to give a white powder (1.36 g, 91 % yield). MP: 230-233 °C ¹H-NMR (D₆-DMSO): 9.78 (2H, s), 7.84 (1H, s), 7.45 (2H, s), 4.49 (4H, br. s), 3.81 (3H, s) ¹³C-NMR (D₆-DMSO): 166, 159, 135, 119, 115, 56 ν_{max} (cm⁻¹): 3323 (br., w), 3301 (br., w), 1643 (m), 1622 (m), 1592 (s), 1535 (m), 1511 (s), 1468 (w), 1452 (w), 1358 (w), 1314 (s), 1285 (m), 1251 (w), 1164 (m), 1131 (w), 1059 (m), 1006 (m), 978 (m), 907 (m), 870 (m), 821 (w), 728 (w), 687 (s), 621 (m), 594 (s), 543 (s), 437 (w) ESI-MS: [C₉H₁₃N₄O₃]⁺ calc. 225.0983, meas. 225.0973

Synthesis of L4

5-Methoxy isophthaloyl hydrazide (500 mg, 2.2 mmol) was stirred in ethanol (40 mL) at room temperature. 2-Acetyl pyrazine (626 mg, 5.1 mmol) was added followed by a catalytic amount of glacial acetic acid. The resulting white suspension was stirred at reflux overnight. After cooling the room temperature, the precipitate was filtered and washed with ethanol (3x5 mL) and diethyl ether (10 mL) to give a white powder (876 mg, 2.0 mmol, 91% yield). MP: >300 °C ν_{max} (cm⁻¹): 3166 (br., w), 3014 (br., w), 2960 (br. w), 1664 (m), 1643 (s), 1596 (w), 1539 (s), 1516 (m), 1496 (m), 1426 (m) 1369 (w), 1338 (s), 1317 (s), 1291 (w), 1254 (s), 1171 (m), 1155 (m), 1141 (m), 1121 (m), 1081 (m), 1047 (m), 1012 (m), 988 (w), 903 (w), 877 (w), 853 (m), 840 (s), 762 (w), 730 (w), 687 (m), 662 (br. m), 572 (w), 478 (w) ESI-MS: [C₂₁H₂₁N₆O³⁺] calc., 433.1732 meas. 433.1738

Synthesis of [Fe₂(L1)₃](BF₄)₂, 1

L1 (15.6 mg, 37.3 μmol) and Fe(BF₄)₂·6H₂O (8.4 mg, 24.9 μmol) were stirred in nitromethane (15 mL) overnight at ambient temperature. The resulting red solution was filtered and vapour diffusion of toluene resulted in red prism crystals suitable for single crystal X-ray diffraction. [Fe₂(C₂₀H₁₉N₉O₂)₃](BF₄)₄·3C₇H₈·29H₂O Found: C, 38.94 H, 3.70 N, 14.72% requires: C, 38.75 H, 5.58 N, 15.07% ν_{max} (cm⁻¹): 3207 (br., w), 1673 (m), 1632 (m), 1598 (s), 1571 (w), 1515 (w), 1492 (s), 1469 (s), 1374 (m), 1343 (w), 1288 (m), 1230 (m), 1190 (m), 1154 (w), 1035 (br., s) 881 (w), 849 (w), 798 (m), 761 (m), 693 (w), 669 (w), 650 (m), 602 (w), 580 (w), 490 (m)

Synthesis of [Fe₂(L2)₃](BF₄)₄, 2

L2 (17.9 mg, 37.3 μmol) and Fe(BF₄)₂·6H₂O (8.4 mg, 24.9 μmol) were stirred in nitromethane (15 mL) overnight at ambient temperature. The resulting red solution was filtered and vapour diffusion of diisopropyl ether resulted in red prism crystals suitable for single crystal X-ray diffraction. [Fe₂(C₂₀H₁₁BrN₈O₂)₃](BF₄)₄·1.5C₆H₁₄O·16H₂O Found: C, 35.99 H, 3.59 N, 14.05% requires: C, 35.35 H, 4.47 N, 14.34% ν_{max} (cm⁻¹): 3623 (br., w), 3249 (br., w), 3077 (w), 2972 (w), 1677 (m), 1598 (w), 1573 (w), 1498 (m), 1474 (m), 1423 (w), 1375 (m), 1341 (w), 1296 (w), 1241 (s), 1193 (m), 1057 (br., s), 931 (w), 901 (m), 844 (w), 808 (m), 762 (m), 736 (w), 689 (m), 651 (w), 602 (w), 556 (m), 519 (m), 474 (m)

Synthesis of [Fe₂(L3)₃](BF₄)₄, 3

L3 (19.7 mg, 37.3 μmol) and Fe(BF₄)₂·6H₂O (8.4 mg, 24.9 μmol) were stirred in acetonitrile (10 mL) for 1 hour to give a dark red-purple solution. The solvent was removed under reduced pressure to give a purple solid. The purple solid was dissolved in nitromethane and stirred at room temperature for 1 hour with a pinch of ascorbic acid. After standing at room temperature for 1 hour the solution was filtered and vapour diffusion of toluene gave dark red block crystals suitable for single crystal X-ray diffraction. [Fe₂(C₂₀H₁₁IN₈O₂)₃](BF₄)₄·2.25C₆H₁₄O·18H₂O Found: C, 34.06 H, 2.89 N, 12.91% requires: C, 33.98 H, 4.60 N, 12.94% ν_{max} (cm⁻¹): 3171 (br., w), 3019 (br., w), 1665 (m), 1646 (s), 1615 (w), 1537 (s), 1516 (m),

1468 (m), 1422 (m), 1369 (w), 1304 (m), 1252 (m), 1171 (s), 1155 (m), 1118 (m), 1073 (m) 1047 (m), 1012 (w), 986 (w), 928 (m), 896 (m), 855 (w), 821 (w), 789 (w), 761 (w), 728 (w), 713 (m), 682 (m), 652 (m), 564 (w), 459 (m)

Synthesis of [Fe₂(L4)₃](BF₄)₂, 4

L4 (16.1 mg, 37.3 μmol) and Fe(BF₄)₂·6H₂O (8.4 mg, 24.9 μmol) were stirred in acetonitrile (10 mL) for 1 hour to give a dark red-purple solution. The solvent was removed under reduced pressure to give a purple solid. The purple solid was dissolved in nitromethane and stirred at room temperature for 1 hour with a pinch of ascorbic acid. After standing at room temperature for 1 hour the solution was filtered and vapor diffusion of diisopropyl ether gave dark red block crystals suitable for single crystal X-ray diffraction [Fe₂(C₂₁H₂₀N₈O₃)₃](BF₄)₄·3C₆H₁₄O·25H₂O Found: C, 38.76 H, 3.86 N, 13.15 requires: C, 38.71 H, 6.10 N, 13.38% ν_{max} (cm⁻¹): 3432 (br., w), 3523 (br., w), 1791 (w), 1663 (s), 1593 (s), 1524 (w), 1499 (w), 1471 (m), 1409 (w), 1375 (m), 1344 (m), 1312 (w), 1284 (w), 1237 (br., m), 1194 (w), 1152 (w), 1054 (br., s), 890 (w), 847 (w), 794 (m), 761 (m), 746 (m), 693 (w), 675 (w), 650 (m), 602 (m), 520 (m), 469 (m)

Acknowledgements

The authors gratefully acknowledge the MacDiarmid Institute for financial support. BHW gratefully acknowledges the receipt of the Roper Scholarship (UC) and the New Zealand-France Friendship Fund for financial support.

Keywords: molecular porous materials • mesocate • Iron(II) • crystal engineering • hydrazone

- [1] (a) Desiraju, G. R., *Curr. Opin. Solid State Mater. Sci.* **1997**, *2*, 451-454; (b) Desiraju, G. R., *Angew. Chem. Int. Ed.* **1995**, *34*, 2311-2327;
- (c) Aakeröy, C. B.; Beatty, A. M., *Aust. J. Chem.* **2001**, *54*, 409-421.
- [2] Su, D.; Wang, X.; Simard, M.; Wuest, J. D., *Supramol. Chem.* **1995**, *6*, 171-178.
- [3] Nugent, P. S.; Rhodus, V. L.; Pham, T.; Forrest, K.; Wojtas, L.; Space, B.; Zaworotko, M. J., *J. Am. Chem. Soc.* **2013**, *135*, 10950-10953
- [4] (a) Han, Y.-F.; Yuan, Y.-X.; Wang, H.-B., *Molecules* **2017**, *22*, 266; (b) He, Y.; Xiang, S.; Chen, B., *J. Am. Chem. Soc.* **2011**, *133*, 14570-14573; (c) H. Wang, B. Li, H. Wu, T.-L. Hu, Z. Yao, W. Zhou, S. Xiang, B. Chen, *J. Am. Chem. Soc.* **2015**, *137*, 9963-9970; (d) Lin, R.-B.; He, Y.; Li, P.; Wang, H.; Zhou, W.; Chen, B., *Chem. Soc. Rev.* **2019**, *48*, 1362-1389; (e) Hisaki, I.; Xin, C.; Takahashi, K.; Nakamura, T., *Angew. Chem. Int. Ed.* **2019**, *58*, 11160-11170; (f) Mastalerz, M.; Oppel, I. M., *Angew. Chem. Int. Ed.* **2012**, *51*, 5252-5255.
- [5] (a) Thomas-Gipson, J.; Beobide, G.; Castillo, O.; Cepeda, J.; Luque, A.; Perez-Yanez, S.; Aguayo, A. T.; Roman, P., *CrystEngComm* **2011**, *13*, 3301-3305; (b) Wilson, B. H.; Scott, H. S.; Qazvini, O. T.; Telfer, S. G.; Mathoniere, C.; Clérac, R.; Kruger, P. E., *Chem. Commun.* **2018**, *54*, 13391; (c) McKeown, N. B., *J. Mater. Chem.* **2010**, *20*, 10588-10597; (d) Sozzani, P.; Comotti, A.; Simonutti, R.; Meersmann, T.; Logan, J. W.; Pines, A., *Angew. Chem. Int. Ed.* **2000**, *39*, 2695-2699; (e) Cooper, A. I., *ACS Central Science* **2017**, *3*, 544-553.
- [6] (a) Tynan, E.; Jensen, P.; Lees, A. C.; Moubarak, B.; Murray, K. S.; Kruger, P. E., *CrystEngComm* **2005**, *7*, 90-95; (b) Tadokoro, M.; Nakasuji, K., *Coord. Chem. Rev.* **2000**, *198*, 205-218; (c) Chowdhry, M. M.; Mingos, D. M. P.; White, A. J. P.; (d) Williams, D. J., *Chem. Commun.* **1996**, 899-900; (e) Natale, D.; Mareque-Rivas, J. C., *Chem. Commun.* **2008**, 425-437; (f) McKay, A. P.; Shillito, G. E.; Gordon, K. C.; McMorran, D. A., *CrystEngComm* **2017**, *19*, 7095-7111; (g) Braga, D.; Maini, L.; Polito,

For internal use, please do not delete. Submitted_Manuscript

FULL PAPER

- M.; Tagliavini, E.; Grepioni, F., *Coord. Chem. Rev.* **2003**, *246*, 53-71; (h) Duong, A.; Maris, T.; Wuest, J. D., *Inorg. Chem.* **2011**, *50*, 5605-5618; (i) Telfer, S. G.; Wuest, J. D., *Cryst. Growth Des.* **2009**, *9*, 1923-1931; (k) Rigby, N.; Jacobs, T.; Reddy, J. P.; Hardie, M. J., *Cryst. Growth Des.* **2012**, *12*, 1871-1881.
- [7] (a) Furukawa, H.; Cordova, K. E.; O'Keeffe, M.; Yaghi, O. M., *Science* **2013**, *341*, 1230444; (b) Hoskins, B. F.; Robson, R., *J. Am. Chem. Soc.* **1989**, *111*, 5962-5964; (c) Li, J.-R.; Kuppler, R. J.; Zhou, H.-C., *Chem. Soc. Rev.* **2009**, *38*, 1477-1504; (d) Tranchemontagne, D. J.; Mendoza-Cortes, J. L.; O'Keeffe, M.; Yaghi, O. M., *Chem. Soc. Rev.* **2009**, *38*, 1257-1283.
- [8] (a) Slater, A. G.; Cooper, A. I., *Science* **2015**, *348*, aaa8075; (b) Feng, S.; Shang, Y.; Wang, Z.; Kang, Z.; Wang, R.; Jiang, J.; Fan, L.; Fan, W.; Liu, Z.; Kong, G.; Feng, Y.; Hu, S.; Guo, H.; Sun, D., *Angew. Chem. Int. Ed.* **2020**, *59*, 3840-3845; (c) Zou, Y.; Ji, X.; Cai, J.; Yuan, T.; Stanton, D. J.; Lin, Y.-H.; Naraghi, M.; Fang, L., *Chem* **2017**, *2*, 139-152.
- [9] Steed, J. W.; Atwood, J. L., *Supramolecular Chemistry*. 2nd Edition ed.; John Wiley & Sons Inc: **2013**.
- [10] (a) Liao, P.-Q.; Chen, X.-W.; Liu, S.-Y.; Li, X.-Y.; Xu, Y.-T.; Tang, M.; Rui, Z.; Ji, H.; Zhang, J.-P.; Chen, X.-M., *Chem. Sci.* **2016**, *7*, 6528-6533; (b) McDonald, T. M.; D'Alessandro, D. M.; Krishna, R.; Long, J. R., *Chem. Sci.* **2011**, *2*, 2022-2028; (c) McDonald, T. M.; Mason, J. A.; Kong, X.; Bloch, E. D.; Gygi, D.; Dani, A.; Crocellà, V.; Giordanino, F.; Odoh, S. O.; Drisdell, W. S.; Vlasisavljevich, B.; Dzubak, A. L.; Poloni, R.; Schnell, S. K.; Planas, N.; Lee, K.; Pascal, T.; Wan, L. F.; Prendergast, D.; Neaton, J. B.; Smit, B.; Kortright, J. B.; Gagliardi, L.; Bordiga, S.; Reimer, J. A.; Long, J. R., *Nature* **2015**, *519*, 303-308; (d) Ma, L.; Falkowski, J. M.; Abney, C.; Lin, W., *Nat. Chem.* **2010**, *2*, 838-846; (b) Yoon, M.; Srirambalaji, R.; Kim, K., *Chem. Rev.* **2012**, *112*, 1196-1231; (e) Zhang, J.; Li, Z.; Gong, W.; Han, X.; Liu, Y.; Cui, Y., *Inorg. Chem.* **2016**, *55*, 7229-7232; (f) Zhu, W.; He, C.; Wu, P.; Wu, X.; Duan, C., *Dalton Trans.* **2012**, *41*, 3072-3077.
- [11] Pham, T.; Forrest, K. A.; Chen, K.-J.; Kumar, A.; Zaworotko, M. J.; Space, B., *Langmuir* **2016**, *32* (44), 11492-11505.
- [12] (a) Cooke, D.J.; Cross, J.M.; Fennessy, R.V.; Harding, L.P.; Rice, C.R.; Slater, C., *Chem. Commun.* **2013**, *49*, 7785-7787; (b) Struch, N.; Brandenburg, J.G.; Schnakenburg, G.; Wagner, N.; Beck, J.; Grimme, S.; Lützen, A., *Eur. J. Inorg. Chem.* **2015**, 5503-5510.
- [13] Van der Sluis, P.; Spek, A. L., *Acta Crystallogr. Sect. A* **1990**, *A46*, 194-201.
- [14] Spek, A. L. PLATON, A Multipurpose Crystallographic Tool, Utrecht University: Utrecht, The Netherlands, **2008**.
- [15] (a) Gilday, L. C.; Robinson, S. W.; Barendt, T. A.; Langton, M. J.; Mullaney, B. R.; Beer, P. D., *Chem. Rev.* **2015**, *115*, 7118-7195; (b) Cavallo, G.; Metrangola, P.; Milani, R.; Pilati, T.; Priimagi, A.; Resnati, G.; Terraneo, G., *Chem. Rev.* **2016**, *116*, 2478-2601.
- [16] Sheldrick, G., *Acta Crystallogr. Sect. A* **2015**, *A71* (1), 3-8.
- [17] Dolomanov, O. V.; Bourhis, L. J.; Gildea, R. J.; Howard, J. A. K.; Puschmann, H., *J. Appl. Crystallogr.* **2009**, *42*, 339-341.
- [18] Sheldrick, G. M. SHELXL-97, Programs for X-ray Crystal Structure Refinement, University of Göttingen, **1997**.
- [19] Song, C.; Ling, Y.; Feng, Y.; Zhou, W.; Yildirim, T.; He, Y., *Chem. Commun.* **2015**, *51* (40), 8508-8511.
- [20] Lifshits, L. M.; Zeller, M.; Campana, C. F.; Klosterman, J. K., *Cryst. Growth Des.* **2017**, *17*, 5449-5457.
- [21] Kraft, A., *J. Chem. Soc., Perkin Trans.* **1999**, *1*, 705-714.
- [22] McCormick, L. J.; Morris, S. A.; Teat, S. J.; McPherson, M. J.; Slawin, A. M. Z.; Morris, R. E., *Dalton Trans.* **2015**, *44*, 17686-17695.
- [23] (a) Kar, P.; Biswas, R.; Drew, M. G. B.; Frontera, A.; Ghosh, A., *Inorg. Chem.* **2012**, *51* (3), 1837-1851; (b) Biswas, C.; Drew, M. G. B.; Escudero, D.; Frontera, A.; Ghosh, A., *Eur. J. Inorg. Chem.* **2009**, *2009*, 2238-2246; (c) Bauzá, A.; Deyà, P. M.; Frontera, A.; Quiñero, D., *Phys. Chem. Chem. Phys.* **2014**, *16*, 1322-1326; (d) Kang, S.-I.; Lee, M.; Lee, D., *J. Am. Chem. Soc.* **2019**, *141*, 5980-5986.

For internal use, please do not delete. Submitted_Manuscript

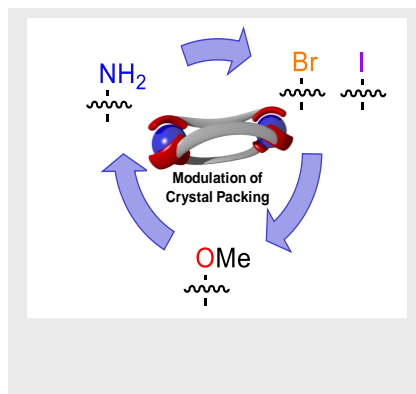
FULL PAPER

Entry for the Table of Contents (Please choose one layout)

Layout 1:

FULL PAPER

A series of dinuclear double mesocates have been prepared with different peripheral functionality on the ligand. In certain cases this pendant functionality - via either the formation of additional supramolecular interactions or an increase in steric bulk - has significant implications for the crystal packing



Benjamin H. Wilson* and Paul E. Kruger*

Page No. – Page No.

Modulation of Crystal Packing via the Tuning of Peripheral Functionality for a Family of Dinuclear Mesocates

Layout 2:

FULL PAPER

((Insert TOC Graphic here; max. width: 11.5 cm; max. height: 2.5 cm))

Author(s), Corresponding Author(s)*

Page No. – Page No.

Title

Text for Table of Contents